Materials Science in Semiconductor Processing 20 (2014) 27–34

Contents lists available at ScienceDirect

Materials Science in Semiconductor Processing

journal homepage: www.elsevier.com/locate/mssp

Annealing effect on structural and optical properties of $Se_{87.5}Te_{10}Sn_{2.5}$ thin films

M.A. Abdel-Rahim [a], A.Y. Abdel-Latief [a], M. Rashad [a,b], N.M. Abdelazim [a,*]

[a] Physics Department, Faculty of Science, Assiut University, Assiut 71516, Egypt
[b] Physics Department, Faculty of Science, Tabuk University, P.O. Box 741, Tabuk, 71491, KSA

ARTICLE INFO

Available online 20 January 2014

Keywords:
Chalcogenide glasses
Optical constants
Thermal differential analysis (DTA)
X-ray diffraction (XRD)
Scanning electron microscopy(SEM)

ABSTRACT

Thin films of $Se_{87.5}Te_{10}Sn_{2.5}$ were prepared by vacuum thermal evaporation technique. Various optical constants were calculated for the studied composition. The mechanism of the optical absorption follows the rule of direct transition. It was found that the optical energy gap (E_g) decreases from 2.26 to 1.79 eV with increasing the annealing temperature from 340 to 450 K. This result can be interpreted by the Davis and Mott model. On the other hand, the maximum value of the refractive index (n) is shifted towards the long wavelength by increasing the annealing temperature. In addition, the high frequency dielectric constant (ε_L) increased from 31.26 to 48.11 whereas the ratio of the free carriers concentration to its effective of mass N/m^* decreased from 4.3 to 2.09 ($\times 10^{57}$ (m^{-3} Kg^{-1})). The influence of annealed temperature on the structure was studied by using the X-ray diffraction (XRD) and scanning electron microscopy (SEM). The XRD studies show that the as-deposited films are amorphous in nature, but the crystallinity improved with increasing the annealing temperature. Furthermore the particle size and crystallinity increased whereas the dislocation and strains decreased with increasing the annealing temperature. SEM examination showed that the annealing temperature induced changes in the morphology of the as-deposited film.

1. Introduction

Chalcogenide glasses are of special interest due to their broad applications in modern electronics, optoelectronics, integrated optics, electro-photography, solar cells, electrical and optical memory devices etc. [1–4]. Among the amorphous chalcogenide alloys mostly selenium (Se) based materials are preferred due to its commercial use. Moreover, its device applications like switching memory and xerography etc., made it attractive. But, the pure Se has a short life time and low sensitivity [5] although is characterized by high viscosity sensitivity. The problem can be overcome by alloying selenium with some impurities such as Ge, Te etc., which in turn gives high crystallization temperature and small aging effects as compared to pure Se glass [6].

Recently, it has pointed out that Se–Te has some advantages over amorphous Se as far as their use in xerography is concerned [7] and the addition of Se to Te alloy improves the corrosion resistance [8]. The Se–Te alloys are found to be useful from the technological point of view if these alloys are thermally stable with time and temperature during use. However, thermal instability leading to crystallization is found to be one of the drawbacks of these alloys. Hence attempt has been made to improve the stability of Se–Te by the addition of third element [9]. The addition of third elements such as Sn to the binary chalcogenide Se–Te system produces stable glassy alloys [10–12]. The insertion of the third element expands the glass forming area and also creates compositional and configurational disorder in the system. It is observed that the addition of the third elements helps in getting cross-linked structure thus increasing the

* Corresponding author. Tel.: +20 1098695542.
E-mail address: nana841@hotmail.co.uk (N.M. Abdelazim).

1369-8001/$ - see front matter © 2014 Elsevier Ltd. All rights reserved.
http://dx.doi.org/10.1016/j.mssp.2013.12.035

glass transition and crystallization temperatures of the binary alloy [11]. There are some characterization studies on several glasses of this Se–Te–Sn system [7,12–17].

This work presents the results of some experimental observation on the effect of heat treatment on structural and optical properties of $Se_{87.5}Te_{10}Sn_{2.5}$ films. Scanning electron microscopy (SEM) and X-ray diffraction were used to determine the structural changes for the studied composition under different conditions. The effect of thermal annealing on optical properties is interpreted according to the density of states model in amorphous materials proposed by Mott and Davis [18].

2. Experimental technique

Bulk $Se_{87.5}Te_{10}Sn_{2.5}$ was prepared by the melt-quench technique. Appropriate amounts of high purity (99.999%) Se, Te and Sn (from Sigma-Aldrich) were weighted (5 g total weight) according to their atomic percentage. The weighted elements were placed into a quartz glass ampoule and sealed under vacuum of 10^{-4} Torr. The sealed ampoule was heated in Heraus programmable tube furnace (type R07115), the heating rate was approximately 3–5 K/min. The temperature was kept at 1100 K for 24 h. The ampoule was manually stirred for realizing the homogeneity of the composition. After that, the ampoule was quenched in an ice-cooled water. Thin films were prepared by thermal evaporation under vacuum of 10^{-5} Torr using Edwards E 306 coating system. A constant evaporation rate (3 nm/s) was used to deposit the films. The evaporation rates as well as the films thickness were controlled using a quartz crystal monitor (FTMS). The film composition was checked using the energy-dispersive spectroscopy (EDAX) technique. The atomic percentage ratio of the films are very close to their initial bulk specimen.

The glassy nature of as-prepared as well as the crystalline phase structures for annealed samples was identified using a Philips diffractometer type 1710. DTA experiments were carried out on the as-prepared powder sample by using a Perkin-Elmer DTG-60 under non-isothermal conditions. The surface morphology of the films was examined using scanning electron microscopy (SEM) Technique Jeol (JSM)-T 200 type. The values of the glass transition temperature (T_g), the onset crystallization temperature (T_c) and the peak crystallization temperature (T_p) were determined with accuracy ± 1 K using the microprocessor of the thermal analyzer. In order to determine the absorption coefficient α and the optical constants of the films as a function of the incident light wavelength, the transmittance $T(\lambda)$ and reflectance $R(\lambda)$ were recorded at room temperature using a double-beam spectrophotometer (Shimadzu uv-2101 combined with pc).

3. Results and discussion

3.1. Structural analysis

A typical DTA traces at different heating rates for $Se_{87.5}Te_{10}Sn_{2.5}$ chalcogenide glass in the temperature range from room temperature to complete crystallization or even melting temperature are shown in Fig. 1. Three characteristic

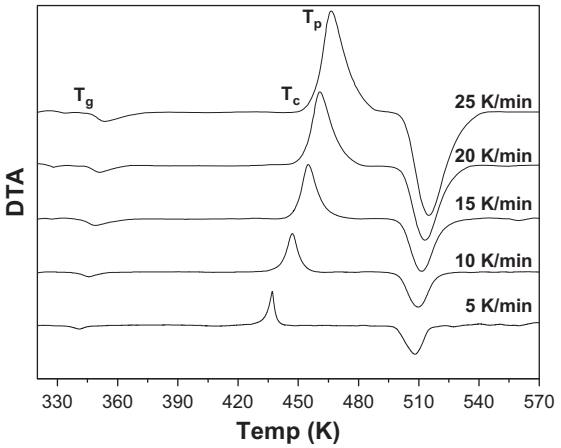

Fig. 1. A typical DTA thermo-gram at different heating rates for $Se_{87.5}Te_{10}Sn_{2.5}$.

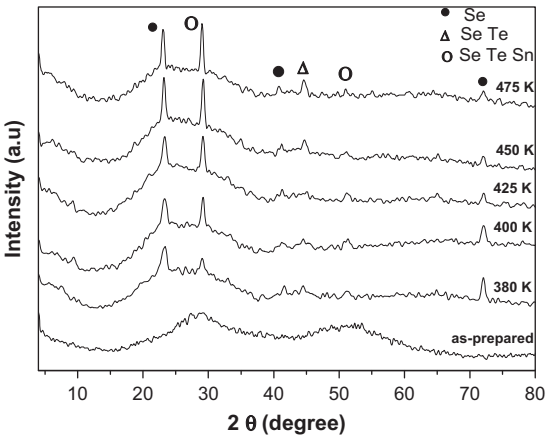

Fig. 2. X-ray diffraction pattern for $Se_{87.5}Te_{10}Sn_{2.5}$ for as-deposited and annealed films at different temperatures for half an hour.

phenomena are clearly observed in the studied temperature region. The first one represents the glass transition region characterized by an endothermic region at the glass transition temperature (T_g). The second one is associated with the crystallization process specified by exothermic peak. The third one is the melting region represented by endothermic reactions. Furthermore, Fig. 1 shows that both the glass transition (T_g) and the crystallization temperature (T_c) shifted to higher temperatures with increasing the heating rates.

In order to determine the crystalline phases for the annealed $Se_{87.5}Te_{10}Sn_{2.5}$ thin films, the X-ray diffraction pattern of films were analyzed. Fig. 2 shows XRD pattern of the as-deposited and annealed $Se_{87.5}Te_{10}Sn_{2.5}$ films. The absence of sharp structural peaks in these patterns confirmed the amorphous (glassy) nature of the sample. However, thin films annealed for 30 min in N_2 atmosphere at 380, 400, 425, 450 and 475 K for half an hour showed a polycrystalline structure indicating an amorphous to crystalline phase transition. The analysis of the XRD patterns for all annealed samples as shown in Fig. 2 show that the

Table 1
The crystallite size (D), strain (ε), and dislocation density (δ) of annealed $Se_{87.5}Te_{10}Sn_{2.5}$ for half an hour at different temperatures.

Phase	Ann. temp. (K)	Crystallite size, D, (nm)	Strain, $\varepsilon \times 10^{-3}$	Dislocation density, $\delta \times 10^{15}$ (m^{-2})
Se	380	10.62	36.6	8.86
	400	11.94	32.7	7.01
	425	15.03	26.1	4.42
	450	21.93	17.8	2.07
	475	22.29	17.5	2.01
Se Te Sn	380	17.13	18.5	3.4
	400	21.49	14.7	2.1
	425	18.8	16.8	2.8
	450	22.95	13.8	1.8
	475	25.54	12.4	1.5

dominant crystalline phases are Se and Se Te Sn. When annealing temperature was further increased to 400 K, the Se and Se Te Sn peaks showed a much greater intensity increase with increasing annealing temperature which indicates a considerable increase in the volume fraction of the two crystalline phases. The average particle size (D) of the annealed samples was calculated from the XRD patterns according to Scherrer's equation [19]

$$D = \frac{k\lambda}{\beta \cos \theta} \tag{1}$$

where k is a constant approximated to unity, its value is related to the particle shape, θ is the diffraction angle, λ is the X-ray wavelength used, β is the width at half maximum intensity (FWHM). The calculated D values using Eq. (1) for the annealed samples are listed in Table 1. On the other hand, the dislocation density (δ) is defined as the length of the dislocation lines per unit volume of the crystal and is given by $(\delta)=1/D^2$. Furthermore, the strain value (ε) is calculated from the following relation [19]:

$$\varepsilon = \left[\frac{\lambda}{D \cos \theta} - \beta\right] \frac{1}{\tan \theta} \tag{2}$$

The deduced δ and ε are listed in Table 1. It is observed that the strain and dislocation density decrease whereas particle size for Se Te Sn and Se phases increases with increasing the annealing temperature, which indicates the improvement in crystallinity of the films. These results are in agreement with the previous work [20–22].

The morphology of the studied composition after annealing at different temperatures for half an hour. The samples were coated with gold before SEM examination to study the surface morphology. The scanning micrograph of the annealed $Se_{87.5}Te_{10}Sn_{2.5}$ composition are shown in Fig. 3(a,b). The microstructure for the annealed samples at 425 K are shown in Fig. 3(a). The surface morphology showed the appearance of a homogeneously distributed dendrite crystalline phase embedded in the glass matrix. Further increase of the annealing reveals that the amount of the transformed crystalline phase increased and the crystallized particles increase in size. This results are in good agreement with the results obtained by XRD. The photomicrograph in Fig. 3(b) shows the surface microstructure of the annealed sample at 475 K for half an hour. A polycrystalline structure in cylindrical shape embedded in an amorphous matrix is observed. Some of these crystallized particles are interconnected and others are isolated. The crystallites are dispersed homogeneously and occupy most of the structure.

3.2. Absorption coefficient

The spectral distribution of transmittance (T) and reflectance (R) as a function of the wavelength for as-prepared and annealed $Se_{87.5}Te_{10}Sn_{2.5}$ films are shown in Figs.4 and 5. It is observed that the transmittance has a maximum and reflectance has a minimum in the range 700–1200 nm. The maximum and minimum may be correlated to each other. In general, it could be noted that the transmittance decreases with increasing the annealing temperature but reflectance shows opposite behavior to this in the transmission spectrum. The optical absorption coefficient (α) was computed from the experimentally measured values of transmittance $T(\lambda)$ and reflectance $R(\lambda)$ according to the following relation [23]:

$$\alpha = \frac{1}{d} \ln\left[\frac{(1-R)^2}{T}\right] \tag{3}$$

where d is the film thickness.

Fig. 6 shows the dependence of the absorption coefficient (α) on the incident photon energy ($h\upsilon$) for as-deposited and annealed $Se_{87.5}Te_{10}Sn_{2.5}$ films. It is observed that the values of the absorption coefficient increase with increasing both photon energy and annealing temperature. In chalcogenide glasses, a typical absorption edge can broadly ascribed to either the three processes (i) residual below-gap absorption, which originates from defects and impurity, (ii) Urbach tail which is strongly related to the structure randomness of the films and (iii) interband absorption, which determined the optical energy gap.

In the high absorption region ($\alpha > 10^4\ cm^{-1}$), a parabolic relation can be applied [24,25]

$$\alpha = \frac{c}{h\upsilon}(h\upsilon - E_g)^r \tag{4}$$

where c is a constant depending on the transition probability, E_g is the optical energy gap of the materials and r is a value depending on the nature of the transition. For a material having one kind of transition, the value of r is 1/2 or 2, for allowed direct or indirect and 3/2 or 3 for forbidden direct or indirect transitions, respectively. The dependency of $(\alpha h\upsilon)^{1/r}$ on photon energy was plotted for

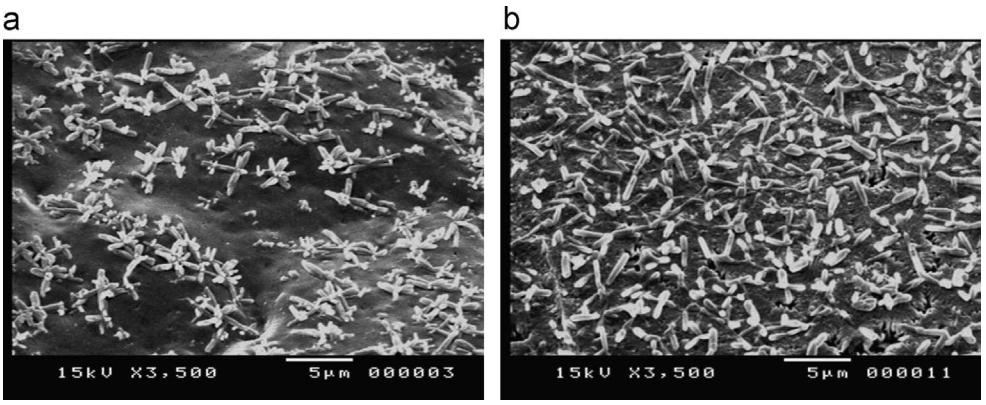

Fig. 3. (a,b) SEM micrographs for annealed $Se_{87.5}Te_{10}Sn_{2.5}$ for half an hour (a) annealed at 425 K and (b) annealed at 475 K for half an hour.

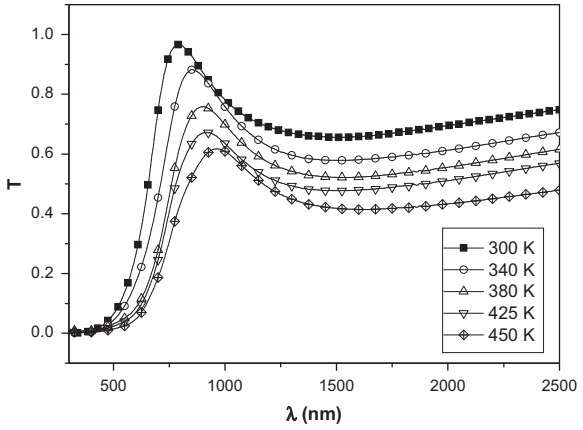

Fig. 4. Spectral dependencies of the transmittance T for as deposited and annealed $Se_{87.5}Te_{10}Sn_{2.5}$ films.

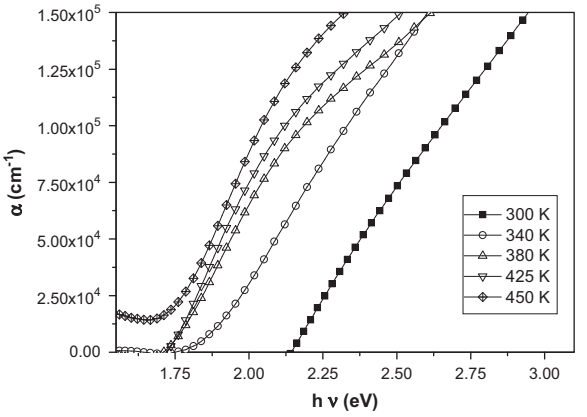

Fig. 6. The absorption coefficient dependence on the photon energy $h\upsilon$ for the as deposited and annealed $Se_{87.5}Te_{10}Sn_{2.5}$ films at different temperatures for half an hour.

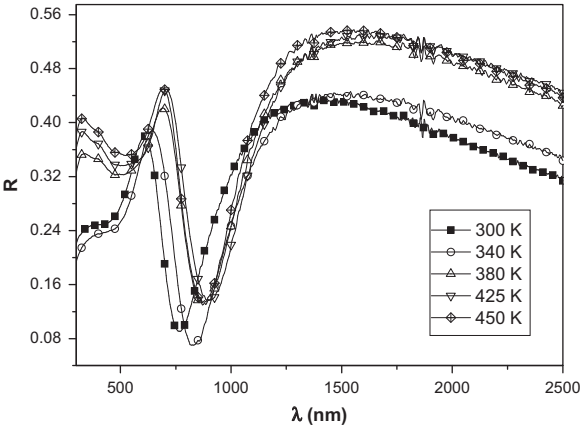

Fig. 5. Spectral dependencies of the reflectance R for as deposited and annealed $Se_{87.5}Te_{10}Sn_{2.5}$ films at different temperatures for half an hour.

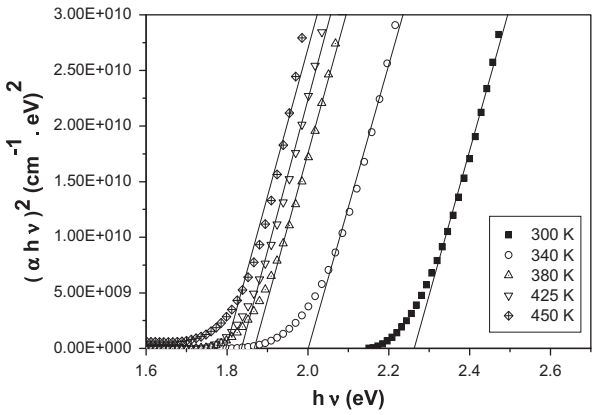

Fig. 7. The dependence of $(\alpha h\upsilon)^2$ on the photon energy for as-deposited and annealed $Se_{87.5}Te_{10}Sn_{2.5}$ films.

different values of r and showed that the transition has a direct allowed nature for the studied composition. It can also be concluded that the relation (4) can be written as

$$(\alpha h\upsilon)^2 = A\,(\hbar\omega - E_g) \tag{5}$$

The linear relationship between $(\alpha h\upsilon)^2$ and $h\upsilon$ for as-deposited and annealed films shown in Fig. 7, confirms direct band gap transition in $Se_{87.5}Te_{10}Sn_{2.5}$ films. These results are in a good agreement with the previous work [22,26]. The intercept with the x-axis gives the direct optical energy gap E_g. The optical energy gap E_g decreases with increasing the annealing temperature as shown in Fig. 8. As the annealing temperature was increased, the

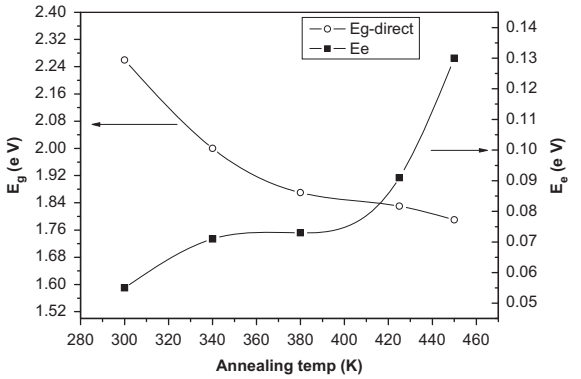

Fig. 8. The variation of optical band gap and the width of localized states versus annealing temperature for the $Se_{87.5}Te_{10}Sn_{2.5}$ films.

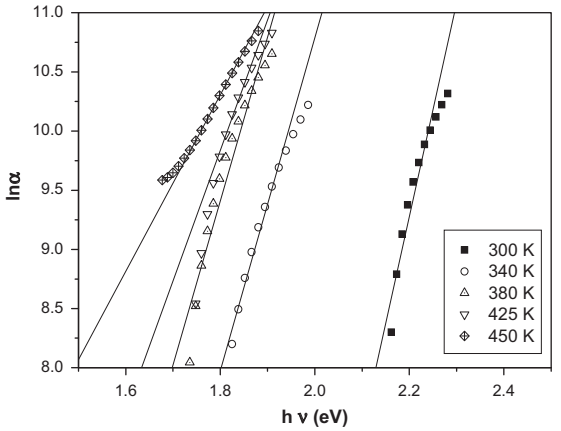

Fig. 9. Plots of ln (α) versus $h\upsilon$ for as-deposited and annealed $Se_{87.5}Te_{10}Sn_{2.5}$ films.

crystallite size increased and the strain value decreased, which leads to decrease in the optical energy gap [27,28].

In the exponential edge region, the absorption coefficient is governed by Urbach's relation [29]

$$\alpha = \alpha_o \exp\left(\frac{h\upsilon}{E_e}\right) \tag{6}$$

where α_0 is a constant and E_e is interpreted as the width of the tails due to localized state in the forbidden gap. Therefore, plotting the dependence of the ln α versus $h\upsilon$ gives a straight line as shown in Fig. 9. The inverse of the slope gives the band tail width (E_e) of the localized states. The effect of annealing temperature on E_e for $Se_{87.5}Te_{10}Sn_{2.5}$ thin films are shown in Fig. 8. It is observed that E_e increases with increasing the annealing temperature. The decrease in the optical energy gap E_g and the increase of localized states tail E_e with the annealing temperature have been successfully analyzed on the basis of the theory proposed by Mott and Davis theory [18]. The thermal annealing above the glass transition temperature T_g is known to be important in including crystallization in semiconducting chalcogenide glasses [30]. The decrease in the optical energy gap E_g and the increase of localized states tails E_e with the annealing temperature can be interpreted by assuming the production of the surface dangling bonds around the crystallites [31] during the process of crystallization. It has been suggested by many authors [31,32] that nearly ideal amorphous solids crystallize under heat treatment and that in the process of crystallization dangling bonds are produced around the surface of the crystallites. Further heat treatment causes the crystallites to break down [33] into smaller crystals thereby increasing the number of surface dangling bonds. These dangling bonds are responsible for the formation of some types of defects in highly polycrystalline solids. As the number of dangling bonds and defects increase with the increase in annealing temperature, the concentration of localized states in the band structure also increases gradually. Hence the heat treatment of the films causes an increase in the energy width of localized states thereby reducing the optical energy gap.

On the other hand, the values of refractive index (n) and extinction coefficient (K_{ex}) have been calculated using the following relations [34,35]:

$$R = \left[(n-1)^2 + K_{ex}^2\right] / \left[(n+1)^2 + K_{ex}^2\right] \tag{7}$$

$$K_{ex} = \frac{\alpha\lambda}{4\Pi} \tag{8}$$

where R is reflectance or reflectivity. The spectral dependence of the refractive index (n) and extinction coefficient (K_{ex}) on the wavelength for as-prepared and annealed $Se_{87.5}Te_{10}Sn_{2.5}$ thin films are shown in Fig. 10(a,b). The values of (n) have a maximum value (n_{max}) at wavelength λ_c which is shifted towards longer wavelength as the annealing temperature increased as shown in Fig. 10(a). Furthermore, the extinction coefficient (K_{ex}) decreases with increasing the wavelength. In general the values of (n) and (K_{ex}) increased with increasing the annealing temperature as shown in Fig. 10(a,b). This type of trend has also been observed for thin films of various other semiconductors [36–39]. The increase of (n) and (K_{ex}) with increasing annealing is caused by an increase in the particle size with annealing temperature [40].

For a better understanding of the optical properties of the as-prepared and annealed films, it is necessary to determine some optical constants such as real (ε_1) and imaginary (ε_2) parts of dielectric constant for as-deposited and annealed $Se_{87.5}Te_{10}Sn_{2.5}$ films, which have been calculated using the relations [41]

$$\varepsilon_1 = n^2 - K_{ex}^2 \quad \text{and} \quad \varepsilon_2 = 2\,n\,K_{ex} \tag{9}$$

The variation of these two parameters with the wavelength is shown in Fig. 11(a,b). On the other hand, the two parameters of the dielectric constant for $Se_{87.5}Te_{10}Sn_{2.5}$ films increase with increasing the annealing temperature.

The dispersion of the refractive index (n) was analyzed using the concept of the single oscillator and can be expressed by the Wimple–Didomenico relationship [42]

$$n^2 - 1 = \frac{E_d E_0}{E_0^2 - E^2} \tag{10}$$

where E_0 is the oscillator energy and considered as an average energy gap, E_d is the dispersion energy which measures the average strength of the interband optical transitions and E is the photon energy.

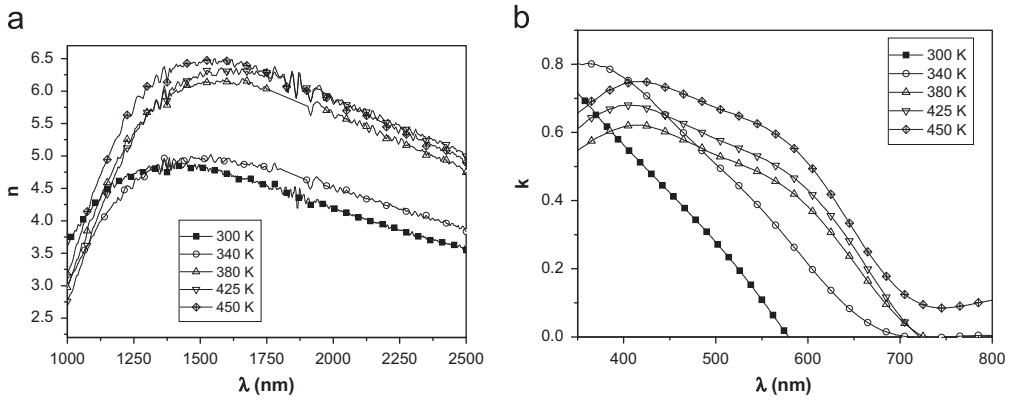

Fig. 10. The variation of (a) refractive index and (b) extinction coefficient with wavelength for as-deposited and annealed $Se_{87.5}Te_{10}Sn_{2.5}$ films.

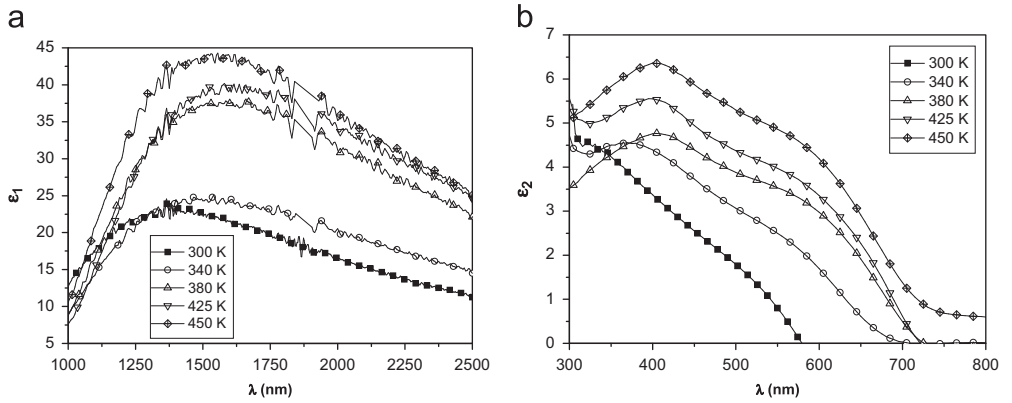

Fig. 11. The variation of (a) real part ε_1 and (b) imaginary part ε_2 with wavelength for as-deposited and annealed $Se_{87.5}Te_{10}Sn_{2.5}$ films.

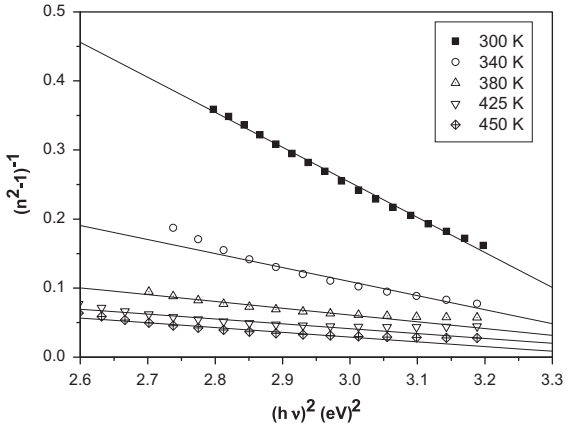

Fig. 12. Plots of $(n^2-1)^{-1}$ versus $(h\nu)^2$ for as-deposited and annealed $Se_{87.5}Te_{10}Sn_{2.5}$ films.

By plotting of $(n^2-1)^{-1}$ versus $(h\nu)^2$ shown in Fig. 12, the dispersion parameter E_d and E_0 can be obtained. The values of E_d and E_0 can be directly determined from the slope and intercept with the vertical axis. The obtained values of E_d and E_0 for the typical $Se_{87.5}Te_{10}Sn_{2.5}$ thin films are listed in Table 2. It is observed that the values of E_d and E_0 nearly increased with increasing the annealing temperature. In our case it is found that $E_0 \approx E_g$ which is in good agreement with the relation of Ticha and Tichy [43]. In general, the increasing E_d and E_0 with the annealing temperature could be attributed to increase the rate of diffusion of atoms of the films with increasing the annealing temperature. The increase in the diffusion rate with increasing temperature gives more number of atoms at interstitial sites, thereby leading to impurity type scattering centers [22,43,44].

Furthermore, in order to calculate the high frequency dielectric constant ε_L we have further analyzed the data of refractive index dependence on photons energy or wavelength via two procedures. The first procedure includes the contribution of free carriers and the lattice vibration modes of dispersion. In this procedure, the relation between the lattice high frequency constant (ε_L) and refractive index (n) is given by the following relation [45]:

$$n^2 = \varepsilon_L - \left(\frac{e^2}{4\,\Pi^2 c^2 \varepsilon_0}\right)\left(\frac{N}{m^*}\right)\lambda^2 \qquad (11)$$

where e is the electronic charge, c is the light velocity, ε_0 is the vacuum permittivity $(8.854\times10^{-12}\ \mathrm{F/m})$, N is the charge carrier concentration and m^* is the effective mass of charge carrier. From the linear plot of n^2 versus λ^2 as shown in Fig. 13 for the studied composition, the lattice dielectric constant ε_L and the ratio of N/m^* for as-prepared

Table 2
The dispersion parameters for as-prepared and annealed $Se_{87.5}Te_{10}Sn_{2.5}$ thin films.

Dispersion parameters	300 K	340 K	380 K	425 K	450 K
E_o (eV)	1.87	1.88	1.91	2.21	2.27
E_d (eV)	1.06	2.57	5.11	7.91	9.5
ε_∞	1.57	2.37	3.68	4.58	4.9
λ_0 (nm)	662.64	659.25	649.03	559.44	545.48
$S_o \times 10^{-6}$(nm)	1.3	3.16	6.3	8.24	8.62
ε_L	31.26	34.38	44.1	46.03	48.11
$N/m^* \times 10^{57}$ (m^{-3} Kg^{-1})	4.3	3.66	3.08	2.93	2.09

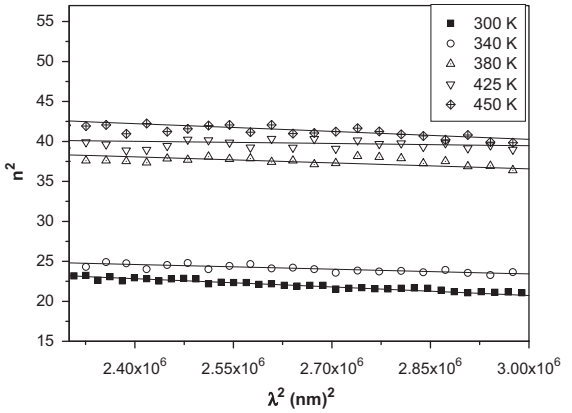

Fig. 13. Plots of n^2 versus λ^2 for as-deposited and annealed $Se_{87.5}Te_{10}Sn_{2.5}$ films.

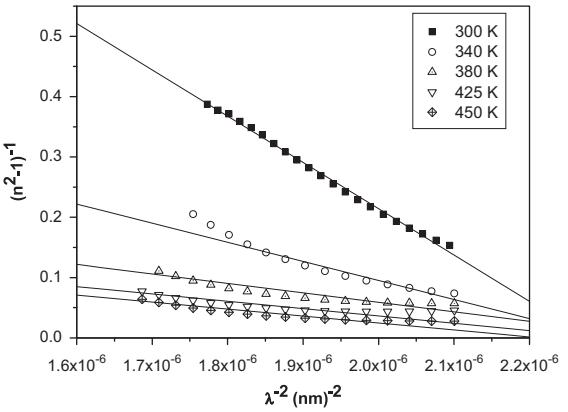

Fig. 14. Plots of $(n^2-1)^{-1}$ versus λ^{-2} for as-deposited and annealed $Se_{87.5}Te_{10}Sn_{2.5}$ films.

and annealed films can be determined. The values of these two parameters with annealing temperature are given in Table 2. It can be seen that the lattice dielectric constant ε_L increases and the ratio N/m^* decreases with increasing the annealing temperature. This behavior was observed in many chalcogenide glasses. In general, it can be concluded that high frequency dielectric constant ε_L and the ratio N/m^* are related to the internal microstructure.

The second procedure for calculating ε_∞ is based upon the dispersion arising from the bound carriers in an empty lattice. In this procedure $\varepsilon_\infty(=n_\infty^2)$ can be calculated by applying the following classical dispersion relation using the single term Sellmeir oscillation [46]:

$$\frac{n_\infty^2-1}{n^2-1}=1-\left(\frac{\lambda_0}{\lambda}\right)^2 \tag{12}$$

where n_∞ is the long wavelength refractive index and λ_0 is the average oscillator wavelength. Plots of $(n^2-1)^{-1}$ versus λ^{-2} for $Se_{87.5}Te_{10}Sn_{2.5}$ thin films are given in Fig. 14. Values of ε_∞ was calculated according to Eq. (12) and listed in Table 2. It is noticed that the values of ε_L are greater than those ε_∞. This behavior can be attributed to the increase in the free carrier concentration [47].

4. Conclusions

From the above results and discussion the following conclusion can be made: the X-ray analysis showed that the as-deposited films have an amorphous nature. Annealing the as-deposited $Se_{87.5}Te_{10}Sn_{2.5}$ films under nitrogen gas showed amorphous to crystalline transition. Furthermore, the average particle size increased whereas the dislocation and strains decreased with increase in annealing temperature. The values of optical band gap (E_g) were found to decrease from 2.25 to 1.75 eV with an increase of annealing temperature from 340 to 450 K. The values of refractive index (n) is shifted towards longer wavelength as the annealing temperature increased, while the extinction coefficient (K_{ex}) decreased with increasing the wavelength. On the other hand, the high frequency dielectric constant (ε_L) increases whereas N/m^* decreases with increasing the annealing temperature.

References

[1] S.R. Ovshinsky, H. Fritzshe, Metall.Trans. 2 (1971) 641.
[2] M.A. Abdel-Rahim, A.H. Moharram, M. Dongol, M.M. Hafiz, J. Phys. Chem. Solids 51 (1990) 355.
[3] M.M. Hafiz, A.H. Moharram, M.A. Abdel-Rahim, A.A. Abu-Sehly, Thin Solid Films 292 (1997) 7.
[4] G. Kaur, T. Komatsu, J. Mater. Sci. 35 (2000) 903.
[5] S.A. Khan, M. Zulfequar, M. Husain, Solid State Commun. 123 (2002) 463.
[6] N. Suri, K.S. Bindra, P. Kumar, R. Thangaraj, J. Non-Cryst. Solids 353 (2007) 264.
[7] M.A. Abdel-Rahim, A. Gaber, A.A. Abu-Sehly, N.M. Abdelazim, Thermochim. Acta 566 (2013) 274.
[8] R. Chiba, N. Funakoshi, J. Non-Cryst. Solids 105 (1988) 149.
[9] N.S. Saxena, J. Non-Cryst. Solids 345 (2004) 161.
[10] G. Kaur, T. Komatsu, R. Thangaraj, J. Mater. Sci. 35 (2000) 903.
[11] N.B. Maharjan, K. Singh, N.S. Saxena, Phys. Status Solidi 195 (2003) 305.
[12] M.A. Abdel-Rahim, A. Gaber, A.A. Abu-Sehly, N.M. Abdelazim, J. Non-Cryst. Solids 376 (2013) 158.
[13] I. Georgieva, D. Nesheva, D. Dimitrov, V. Kozhukharov, J. Non-Cryst. Solids 160 (1993) 105.

[14] F. Abdel-Wahab, Physica B 406 (2010) 1053.
[15] S. Kumar, G.B.V.S. Laxmi, M. Husain, M. Zulfequar, Eur. Phys. J. Appl. Phys. 35 (2006) 155.
[16] V. Sharma, A. Thakur, J. Sharma, V. Kumar, S. Gautam, S.K. Tripathi, J. Non-Cryst. Solids 353 (2007) 1474.
[17] V.K. Saraswat, V. Kishore, D.K. Sharma, N.S. SaxenaT.P. Sharma, Chalcogenide Lett. 4 (2007) 61.
[18] N. Mott, E. Davis, Electronic Process in Non-Crystalline Materials, Clarendon Press, Oxford, 1971.
[19] A.J.P. Wilson, Mathematical Theory of X-ray Powder Diffractometry, Cordon and Breach, New York, 1963.
[20] M.A. Abdel-Rahim, A. El-Korashy, S. Al-Ariki, Mater. Trans. 51 (2) (2010) P256.
[21] A. Aytunc, M. Kundaka, A. AstamM. Yildirm, Physica E 40 (2008) 2709.
[22] M.A. Abdel-Rahim, M.M. Hafiz, A. Elwab, B. Alwany, Opt. Laser Technol. 44 (2012) 1116.
[23] M. El-Nahass, Opt. Laser Technol. 39 (2007) 347.
[24] M.A. Abdel-Rahim, J. Phys. Chem. Solids 60 (1999) 29.
[25] E.A. Davis, N.F. Mott, Philos. Mag. 22 (1970) 903.
[26] V.K. Saraswat, V. Kishore, Chalcogenide Lett. 4 (2007) 61.
[27] S. Venkatachalam, D. MangalorajSa.K. Narayandass, Physica B 47 (2007) 393.
[28] K.B. Kale, C.D. Lokhande, Appl. Surf. Sci. 252 (2005) 929.
[29] F. Urbach, Phys. Rev. 92 (1953) 1324.
[30] M.A. Abdel-Rahim, A.Y. Abdel-latief, A. El-Korashy, M.A. Sabet, Mater. Trans. 51 (3) (2010) 428.
[31] S. Chaudhri, S.K. Biswas, J. Non-Cryst. Solids 54 (1983) 179.
[32] S.A. Khan, M. ZulfequarM. Husain, Physica B 324 (2002) 336.
[33] S. Hasegawa, M. Kitagawa, Solid State Commun. 27 (1978) 855.
[34] O.S. Heavens, Optical Properties of Thin Films, Dover Publications, New York, 1965.
[35] P. Sharma, V. Sharma, S.C. Katyal, Chalcogenide Lett. 3 (2006) 73.
[36] M.A. Abdel-Rahim, M.M. Hafiz, M.M. El-Nahass, A.M. Shamekh, Physica B 327 (2007) 383.
[37] H. Mahfoz Kotb, M.A. Dabban, A.Y. Abdel-Latif, M.M. Hafiz, J. Alloys Compd. 512 (2012) 115.
[38] M.A. Abdel-Rahim, M.M. Hafiz, A. Elwhab, B. Alwany, Opt. Laser Technol. 47 (2013) 88.
[39] F.S. Al-Hazmi, Physica B 404 (2009) 1354.
[40] E. Bertan, A. Lousa, Sol. Energy Mater. 17 (1988) 55.
[41] F. Tepehan, N.Ozer, Sol. Energy Mater. Sol. Cells 30 (1993) 353.
[42] S.H. Wemple, Phys. Rev. B7 (1973) 3767.
[43] H. TichaL. Tichy, J. Optoelectron. Adv. Mater. 4 (2002) 381.
[44] M.M. Malik, M. Zulfequar, A. Kumar, M. Husain, J. Phys. Condens. Matter 4 (1992) 8331.
[45] J.N. Zemel, J.D. Jensen, R.B. Schoolar, Phys. Rev. A140 (1963) 330.
[46] A.K. Wolaton, T.S. Moss, Proc. R. Soc. 81 (1961) 5091.
[47] F. Yakuphanogla, C. Viswanthan, J. Non-Cryst. Solids 353 (2007) 2934.